

Spintronic properties of one-dimensional electron gas in graphene armchair ribbons

J. W. Lee, S. C. Kim, and S. -R. Eric Yang*
Physics Department, Korea University, Seoul 136-701, Korea

We have investigated, using effective mass approach (EMA), magnetic properties of a one-dimensional electron gas in graphene armchair ribbons when the electrons occupy only the lowest conduction subband. We find that magnetic properties of the one-dimensional electron gas may depend sensitively on the width of the ribbon. For ribbon widths $L_x = 3Ma_0$, a critical point separates ferromagnetic and paramagnetic states while for $L_x = (3M + 1)a_0$ paramagnetic state is stable (M is an integer and a_0 is the length of the unit cell). These width-dependent properties are a consequence of eigenstates that have a subtle width-dependent mixture of \mathbf{K} and \mathbf{K}' states, and can be understood by examining the wavefunction overlap that appears in the expression for the many-body exchange self-energy. Ferromagnetic and paramagnetic states may be used for spintronic purposes.

PACS numbers:

I. INTRODUCTION

Generation of spin-polarized current is of significant importance both scientifically and technologically. A spin-polarized current would emerge naturally from ferromagnetic materials. In order to achieve a spintronic device, it is important to find non-magnetic materials where a spin-polarized current can be flowed without becoming depolarized. It has become possible to induce and detect spin polarization in non-magnetic semiconductors[1–3]. In this paper we explore the possibility that graphene[4] field effect transistors[5] based on armchair nanoribbons can be used to generate spin-polarized currents. The conduction electrons in carbon-based materials can move very long distances without scattering due to their small spin-orbit coupling and low hyperfine interaction. Recently magnetic effects using graphene edges states of an armchair ribbon have been explored[6]. In our work we investigate bulk magnetic properties of a one-dimensional electron gas of armchair ribbons, where electrons interact via long-range Coulomb interaction. It is possible that a ferromagnetic state may be stable in such a system as the investigation of one-dimensional Hubbard model with nearest neighbor electron-electron interaction suggests[7].

Graphene armchair ribbons[8–10] have several special properties that are well suited for spintronic applications. According local density approximation (LDA) when the width of an armchair ribbon is $L_x = 3(M + 1)a_0$ or $L_x = 3Ma_0$ a gap exists in the energy spectrum [9] (a rather small gap exists when $L_x = (3M + 2)a_0$, and this case will not be considered here). The other property is that boundary condition on the armchair edges admix \mathbf{K} and \mathbf{K}' valleys, and eigenstates are mixture of \mathbf{K} and \mathbf{K}' states forming one-dimensional subbands[10] (this is in contrast to parabolic and cylindrical potentials[11–13],

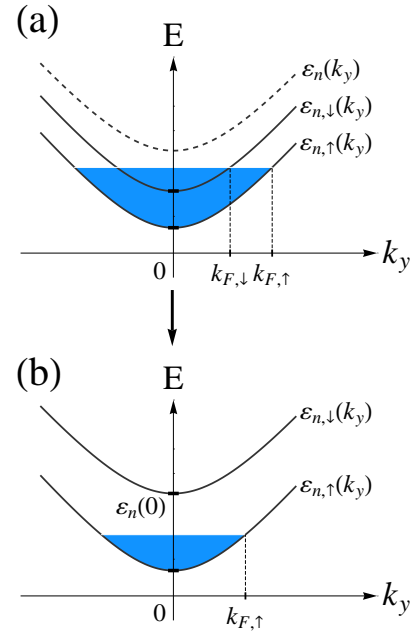


FIG. 1: (a) Electron density is such that the exchange self-energy is smaller than the Fermi energy and the electron gas is partially spin-polarized. We assume that, among conduction subbands, only the lowest energy conduction subband is occupied with electrons. Dashed line indicates spin degenerate subband energy in the absence of electron-electron interactions. Spin-up and -down subbands are shown. (b) For a smaller electron density the exchange self-energy can be larger than the Fermi energy and the electron gas is fully spin-polarized.

where the mixing is rather small). When the system is doped electrons occupy these subbands and a one-dimensional electron gas forms, see Fig.1. The other unique property is a rather small value of the dielec-

*corresponding author, eyang812@gmail.com

tric constant ($\epsilon \sim 1$), which makes effects of Coulomb interaction effects strong. Many-body self-energies are thus one order of magnitude larger in comparison to the corresponding values of an electron gas of ordinary semiconductors with $\epsilon \sim 10$.

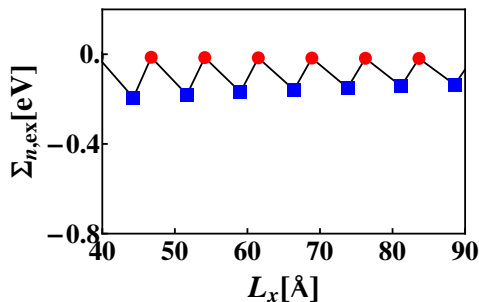


FIG. 2: Exchange self energies of doped graphene for ribbon widths $L_x = 3(M+1)a_0$ (circles) and $L_x = 3Ma_0$ (squares), where $a_0 = 2.46\text{\AA}$ and M is an integer. The effective mass approach is used. Here the dielectric constant is $\epsilon = 3$ and the dimensionless Fermi wavevector is $k_F a_0 = 0.07$.

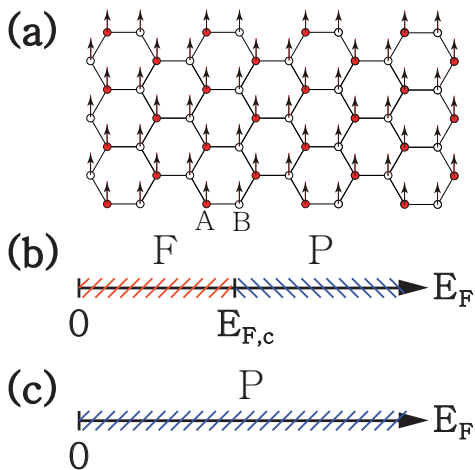


FIG. 3: (a) Bulk ferromagnetic state of one-dimensional electron gas in a graphene armchair ribbon. We assume that only the conduction subband of a graphene armchair ribbon that is closest in energy to $E = 0$ is occupied. The average spin value per carbon site is shown as vertical arrows (Only spins of electrons belonging to the lowest conduction subband are shown). (b) Phase diagram as a function of the Fermi energy E_F for the length of ribbon $L_x = 3Ma_0$. E_F is measured from the bottom of the conduction subband. F (P) stands for ferromagnetic (paramagnetic) state. (c) Phase diagram for $L_x = (3M+1)a_0$.

In this work we assume that a gap separates conduction and valence subbands, and that, among conduction subbands, only the lowest energy conduction subband is occupied with electrons. We calculate the many-body exchange self-energy Σ_{ex} of a spin-polarized one-dimensional electron gas of such a system for relatively

large values of the width $L_x \geq 45\text{\AA}$, where the LDA and EMA results agree approximately (see Sec.II). The width dependence of Σ_{ex} is shown in Fig.2. Using these results we find that, for ribbon widths $L_x = 3Ma_0$, a critical point separates ferromagnetic and paramagnetic states while paramagnetic state is stable for $L_x = (3M+1)a_0$. These results are illustrated in Fig.3. This dependence on the width can be understood by examining the wavefunction overlap that appears in the expression for the exchange self energy. The effect is a consequence of eigenstates that have a subtle width-dependent mixture of \mathbf{K} and \mathbf{K}' states. The large difference in the values of dielectric constants of graphene and ordinary semiconductors cannot explain these width-dependent magnetic properties.

II. EFFECTIVE MASS APPROXIMATION AND MODEL HAMILTONIAN

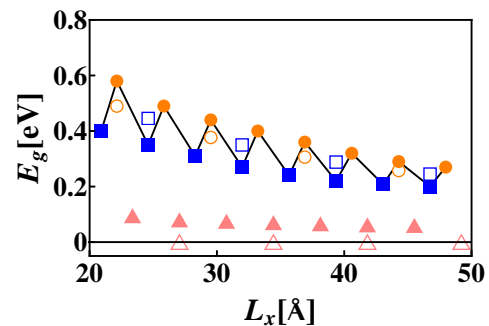


FIG. 4: Size of gap E_g of undoped graphene is shown. LDA results[9] for widths $L_x = 3(M+1)a_0$ (filled circles), $L_x = 3Ma_0$ (filled squares), and $L_x = 3(M+2)a_0$ (filled triangles). EMA results for the same widths are open squares, circles, and triangles.

Effective mass approach can describe numerous physical properties of graphene approximately. It can be derived from tight binding method[14]. Fig.4 displays the value of the gap of armchair ribbons as a function of the width. Both LDA[9] and EMA results are shown for *undoped* armchair ribbons. We see that the LDA values of the magnitude of the gap are in rough agreement with those of the EMA results, and the agreement becomes better for larger values of L_x . However, there are several deviations. The EMA value of the gap is zero for $L_x = (3M+2)a_0$ while that of LDA is small but non-zero. Also as L_x changes between $3(M+1)a_0$ and $3Ma_0$ the LDA value of the gap displays small oscillations while the EMA results do not. LDA includes electron-electron interaction effects and goes beyond nearest neighbor hopping while EMA does not. However, when L_x is larger than 45\AA and $L_x = 3(M+1)a_0$ or $L_x = 3Ma_0$ the EMA results are approximately correct. We will employ EMA to compute the approximate exchange self energy under these conditions.

We choose \mathbf{K} and \mathbf{K}' valleys as $\mathbf{K} = \frac{2\pi}{a_0}(\frac{1}{3}, \frac{1}{\sqrt{3}})$ and $\mathbf{K}' = \frac{2\pi}{a_0}(-\frac{1}{3}, \frac{1}{\sqrt{3}})$. The ribbon is along y-axis. The envelope wavefunctions $[\psi_A, \psi_B,]$ and $[\psi'_A, \psi'_B]$ can be combined into $\Psi = (\psi_A, \psi_B, -\psi'_A, -\psi'_B)$, which satisfies the Hamiltonian

$$H_0 = \gamma a_0 \begin{pmatrix} 0 & \mathbf{k}_x - i\mathbf{k}_y & 0 & 0 \\ \mathbf{k}_x + i\mathbf{k}_y & 0 & 0 & 0 \\ 0 & 0 & 0 & -\mathbf{k}_x - i\mathbf{k}_y \\ 0 & 0 & -\mathbf{k}_x + i\mathbf{k}_y & 0 \end{pmatrix}. \quad (1)$$

Wavevector $k_{x,y}$ is measured from \mathbf{K} and \mathbf{K}' in the upper and lower Hamiltonians, respectively. The hard wall boundary conditions[15] on each of the total A and B components of the wavefunction at the armchair edges $x = 0$ and $x = L'_x = L_x + a_0$ admix \mathbf{K} and \mathbf{K}' valleys. Note that envelope wavefunctions along the x-axis are $e^{\pm ik_n x}$ and have the opposite wavevectors k_n and $-k_n$ for \mathbf{K} and \mathbf{K}' . The wavefunction Ψ of conduction subbands are[10]

$$\Psi_n(x, y, k_y) = \frac{e^{ik_y y} \theta(x)}{2\sqrt{L'_x} \sqrt{L_y}} \begin{pmatrix} -e^{-i\theta_{k_n, k_y}} e^{ik_n x} \\ e^{ik_n x} \\ -e^{-i\theta_{k_n, k_y}} e^{-ik_n x} \\ e^{-ik_n x} \end{pmatrix}, \quad (2)$$

where $\theta(x) = 1$ for $0 \leq x \leq L'_x$ and 0 otherwise. The wavevector of the n'th subband is $k_n = \frac{n\pi}{L_x} - \frac{2\pi}{3a_0}$ and $\theta_{k_n, k_y} = \text{Arctan}(k_y/k_n)$. The eigenenergy is $\epsilon_n(k_y) = \gamma a_0 \sqrt{k_y^2 + k_n^2}$, where $\gamma = \frac{\sqrt{3}}{2}t$ and $t = 2.7\text{eV}$. Subband energies near $E = 0$ are plotted in Fig.5 for two possibilities $L_x = 3Ma_0$ and $L_x = (3M+1)a_0$. In this figure the value of L_x is chosen so that in the first case $k_n > 0$ while in the second case $k_n < 0$.

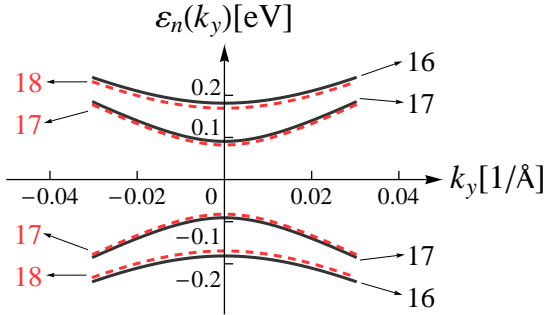


FIG. 5: Conduction and valence subbands with energies closest near $E = 0$. Solid lines are for $L_x = 3Ma_0 = 24a_0$. Dashed lines are for $L_x = (3M+1)a_0 = 25a_0$. The numbers beside the curves indicate values of subband index n .

III. EXCHANGE SELF-ENERGY

We consider spin-polarized electrons in the lowest energy conduction subband with the electron density $n_D =$

$\frac{k_F}{\pi}$, where k_F is the Fermi wavevector. In our model, we ignore the inter-subband mixing by Coulomb interaction, which is a standard approximation[16]. Then Hartree-Fock *self-consistent* eigenfunctions are *plane waves*[17], given by Eq.(2), and no corrections of the kinetic energy are present. Note the Hartree self-energy will cancel with the potential of uniform positive background.

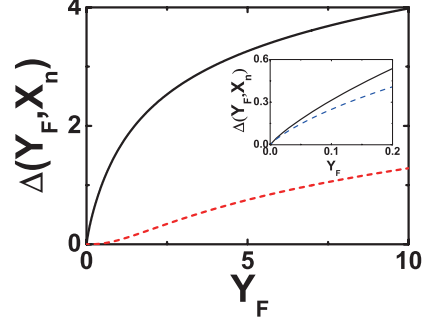


FIG. 6: Magnitude of dimensionless exchange self-energy $\Delta(Y_F, X_n)$ as a function of Y_F for $X_n = \pi/3$ (solid line) and $-\pi/3$ (dashed line). Inset: magnitude of the dimensionless self-energy $\Delta(Y_F, X_n)$ as a function of Y_F computed using Eq.(4) (solid line) and Eq.(5) (dashed line) for $X_n = \pi/3$.

We denote these wavefunctions by $|k_y\rangle$. At $k_y = 0$ the exchange self-energy[17] is

$$\Sigma_{n,ex}(0) = -\frac{L_y}{2\pi} \int_{-k_F}^{k_F} dk_y \left\langle 0, k_y \left| \frac{e^2}{\epsilon|\mathbf{r}_1 - \mathbf{r}_2|} \right| k_y, 0 \right\rangle, \quad (3)$$

which can be written as $\Sigma_{n,ex}(0) = -\frac{e^2}{\epsilon L'_x} \Delta(Y_F, X_n)$ with the dimensionless exchange self-energy defined as

$$\begin{aligned} \Delta(Y_F, X_n) &= \frac{1}{2\pi} \int_{-\infty}^{\infty} dX \int_{-Y_F}^{Y_F} dY \left(1 + \frac{X_n}{\sqrt{X_n^2 + Y^2}} \right) \frac{(1 - \cos X)}{\sqrt{X^2 + Y^2} X^2}. \end{aligned} \quad (4)$$

Here $Y = k_y L'_x$, $Y_F = k_F L'_x$ and $X_n = k_n L'_x$ are all dimensionless. In the case $L_x = 3Ma_0$ we have $X_n = \pi(n - 2M - \frac{2}{3})$, and the conduction subband with the *lowest energy* has the value $X_n = \pi/3$ corresponding to the value $n = 2M+1$. For $L_x = (3M+1)a_0$ we have $X_n = \pi(n - 2M - \frac{4}{3})$, and the conduction subband with the *lowest energy* has the value $X_n = -\pi/3$ corresponding to $n = 2M+1$. In Fig.6 $\Delta(Y_F, X_n)$ is plotted as a function of Y_F for $X_n = \pi/3$ and $-\pi/3$. For $Y_F \ll 1$ we can approximate

$$\begin{aligned} \Delta(Y_F, X_n) &\simeq (1/\pi) \left(1 + \frac{X_n}{\sqrt{X_n^2 + Y_F^2}} \right) \left(\frac{-2}{Y_F^3} \right) \\ &\times \left(Y_F^2 + 2 G_{1,3}^{2,1} \left(\begin{matrix} 5/2 \\ 1, 2, 3/2 \end{matrix} \middle| \frac{Y_F^2}{4} \right) \right) \end{aligned} \quad (5)$$

where G is Meijer G-function[18]. In Fig.6 this approximate analytical result is compared with the exact numerical result of Eq.(4). As expected, the agreement between the two are excellent for small values of Y_F .

Exchange self energies of doped graphene for ribbon widths $L_x = 3(M+1)a_0$ and $L_x = 3Ma_0$ are shown in Fig.2. Here the dimensionless Fermi wavevector $k_F a_0 = 0.07$. We notice that the self energy displays oscillations as L_x changes between $3(M+1)a_0$ and $3Ma_0$. A similar effect was *also* observed in the LDA result for the gap in the undoped case (compare Figs.2 and 4).

Spontaneous spin splitting will occur in the lowest conduction subband when $|\Sigma_{n,ex}(0)| > E_F$, see Fig.1. This condition is equivalent to $\frac{e^2}{\epsilon\gamma a_0}\Delta(Y_F, X_n) > \sqrt{X_n^2 + Y_F^2} - |X_n|$. At $X_n = \pi/3$ the inequality is satisfied when $Y_F < 11.309$ for $\epsilon = 1$ and $Y_F < 3.22$ for $\epsilon = 3$. The critical point between ferromagnetic and paramagnetic states is shown schematically in Fig.3(b). At $X_n = -\pi/3$ no critical point exists since $\Delta(Y_F, X_n)$ is too small, see Fig.6. In this case paramagnetic state is stable, as illustrated in Fig.3(c).

Also we must require that the exchange self energy correction be smaller than the gap $|\Sigma_{n,ex}(0)| < E_g = 2\gamma a_0 |k_n|$. This condition is equivalent to $\frac{e^2}{\epsilon\gamma a_0}\Delta(Y_F, X_n) < 2|X_n| = \frac{2\pi}{3}$. We find at $X_n = \pi/3$ that this condition is satisfied when $Y_F < 0.364$ for $\epsilon = 1$ and $Y_F < 2.439$ for $\epsilon = 3$.

The dependence on the width can be understood by examining the wavefunction overlap that appears in the expression for the exchange self energy. It is given by $|\psi_n^*(x, y, 0)\psi_n(x, y, k_y)|^2 \propto 1 + \cos\theta_{k_n, k_y}$ for $\mathbf{r}_1 = \mathbf{r}_2$. When $k_n < 0$ the quantity $\cos\theta_{k_n, k_y} = \frac{X_n}{\sqrt{X_n^2 + Y^2}} < 0$, which makes the dimensionless self energy $\Delta(Y_F, X_n)$ smaller, see the integrand in Eq.(4). This effect is a consequence of the presence of the phase factors $e^{-i\theta_{k_n, k_y}}$ only in certain components of the eigenstate wavefunctions (see Eq.(2)) and that the value of k_n for the lowest conduction subband is *negative* when $L_x = (3M+1)a_0$ (see arguments below Eq.(4)). In other words it is a consequence of a subtle width-dependent mixture of \mathbf{K} and \mathbf{K}' states in the eigenstate wavefunctions.

IV. SUMMARY AND DISCUSSIONS

As the comparison with the LDA result shows, when L_x large and for $L_x = 3(M+1)a_0$ and $L_x = 3Ma_0$ the

result of EMA is approximately correct. *Under* these conditions we have employed EMA to compute the approximate exchange self energy. We have shown that when *only* the lowest conduction subband of a graphene armchair ribbon is occupied magnetic properties of the one-dimensional electron gas may depend sensitively on the width of the ribbon. We find that, for ribbon widths $L_x = 3Ma_0$, a critical point separates ferromagnetic and paramagnetic states while paramagnetic state is stable for $L_x = (3M+1)a_0$. This dependence is in sharp contrast to one-dimensional electron gas of ordinary semiconductors, and can be understood by examining the wavefunction overlap that appears in the expression for the exchange self energy of an armchair ribbon. It reflects the fact that eigenstate wavefunctions of an armchair ribbon contain a non-trivial width-dependent mixture of \mathbf{K} and \mathbf{K}' states. The large difference in the value of dielectric constant between graphene and ordinary semiconductors alone cannot explain our width-dependent magnetic properties. The magnitude of the exchange spin splitting is of order $\frac{e^2}{\epsilon L_x}$, and, depending on the size of the Fermi wavevector k_F , it can vary in the range of 10 – 100meV. As shown in Fig.1 our work suggests that the degree of spin polarization in a graphene armchair ribbon may be controlled by changing the gate voltage.

An estimation, using the usual mean field value, gives that Curie temperature $k_B T_c$ is of the order of the exchange self energy 0.1eV. However, quantum fluctuations may reduce this value. A spin-polarized CDW and a Luttinger liquid are possible true groundstates. It may be worthwhile to investigate these issues using improved approximation schemes than EMA employed in this paper, such as spin density functional method and exact diagonalization techniques. Our results suggest that experimental investigations of magnetism in one dimensional electron gas of an armchair ribbon may produce numerous interesting results.

Acknowledgments

We thank A.H. MacDonald for several useful suggestions. This research was supported by Basic Science Research Program through the National Research Foundation of Korea(NRF) funded by the Ministry of Education, Science and Technology (2012R1A1A2001554).

-
- [1] B. V. Wees, Nature Phys. **3**, 147 (2007).
 [2] S. P. Dash, S. Sharma, R. S. Patel, M. P. de Jong, and R. Jansen, Nature **462**, 491 (2009).
 [3] S.-R. Eric Yang and A. H. MacDonald, Phys. Rev. B **67**, 155202 (2003).
 [4] A. K. Geim and A. H. MacDonald, Phys. Today, **60**, 35

- (2007).
 [5] F. Schwierz, Nat. Nanotechnol. **5**, 487 (2010).
 [6] H.-H. Lin, T. Hikihara, H.-T. Jeng, B.-L. Huang, C.-Y. Mou, and X. Hu, Phys. Rev. B **79**, 035405 (2009). In this work the edges states that are responsible for magnetism are partially filled. In our case these edge states are either

- empty or completely filled and are not relevant.
- [7] S. Daul and R.M. Noack, *Z. Phys.B* **103**, 293 (1997); R. Strack, D. Vollhardt, *J. Low Temp. Phys.* **99**, 385 (1995). In one-dimensional Hubbard model the ferromagnetic state is unstable when only the on-site (short-range) interaction is used. However, Strack and Vollhardt demonstrate that the ferromagnetic state can become stable when the *nearest* neighbor Coulomb interaction is included.
- [8] A. H. Castro Neto, F. Guinea, N. M. R. Peres, K. S. Novoselov, and A. K. Geim, *Rev. Mod. Phys.* **81**, 109 (2009).
- [9] Y.-W. Son, M. L. Cohen, and S. G. Louie, *Phys. Rev. Lett.* **97**, 216803 (2006).
- [10] L. Brey and H. A. Fertig, *Phys. Rev. B* **73**, 235411 (2006).
- [11] P. S. Park, S.C. Kim, and S.-R. Eric Yang, *Phys. Rev. Lett.* **108**, 169701 (2012).
- [12] P.S. Park, S.C. Kim, and S.-R. Eric Yang, *J. Phys.: Condens. Matter* **22**, 375302 (2010); P.S. Park, S.C. Kim, and S.-R. Eric Yang, *Phys. Rev. B* **84**, 085405 (2011).
- [13] S.C. Kim, and S.-R. Eric Yang, *J. Phys.: Condens. Matter* **24**, 195301 (2012).
- [14] T. Ando, *J. Phys. Soc. Jpn.* **74**, 777 (2005).
- [15] C. Tang, W. Yan, Y. Zheng, G. Li, and L. Li, *Nanotechnology* **19**, 435401 (2008); S.C. Kim, P.S. Park, and S.-R. Eric Yang, *Phys. Rev. B* **81**, 085432 (2010).
- [16] H. Haug and S. W. Koch, *Quantum theory of the optical and electronic properties of semiconductors* (World Scientific, Singapore, 1990).
- [17] N. W. Ashcroft and N. D. Mermin, *Solid State Physics* (Brooks Cole, 1976).
- [18] H. Bateman and A. Erdlyi, *Higher Transcendental Functions*, Vol. I. (McGrawHill, New York, 1953).